Macula Vessel Density and Foveal Avascular Zone Parameters in Exfoliation Glaucoma Compared to Primary Open-Angle Glaucoma

Shawn Philip,[1] Ahmad Najafi,[1] Apichat Tantraworasin,[2] Toco Y. P. Chui,[1] Richard B. Rosen,[1] and Robert Ritch[1]

[1]Einhorn Clinical Research Center, Department of Ophthalmology, New York Eye and Ear Infirmary of Mount Sinai, New York, New York, United States
[2]Clinical Epidemiology and Statistics Unit and Department of Surgery, Faculty of Medicine, Chiang Mai University, Chiang Mai, Thailand

Correspondence: Ahmad Najafi, New York Eye and Ear Infirmary of Mount Sinai, 310 East 14th Street, Suite 500, New York, NY 10003, USA; anajafi@mountsinai.org.

SP and AN contributed equally to the work presented here and should therefore be regarded as equivalent authors.

Submitted: October 17, 2018
Accepted: February 20, 2019

Citation: Philip S, Najafi A, Tantraworasin A, Chui TYP, Rosen RB, Ritch R. Macula vessel density and foveal avascular zone parameters in exfoliation glaucoma compared to primary open-angle glaucoma. *Invest Ophthalmol Vis Sci*. 2019;60:1244–1253. https://doi.org/10.1167/iovs.18-25986

Purpose. The purpose of this study was to explore macula vessel density and foveal avascular zone (FAZ) parameters in exfoliation glaucoma (XFG) compared to primary open-angle glaucoma (POAG) using optical coherence tomography angiography (OCTA).

Methods. This was a cross-sectional observational study. Twenty-six XFG and 28 POAG patients with comparable visual field defects on Humphrey 24-2 and 10-2 perimetries were recruited. OCTA scans (3 × 3 mm) centered on the fovea were obtained. Built-in software was used to measure superficial capillary plexus (SCP) vessel density at different quadrants of the macula. Custom software was then used to create a full-thickness image. The FAZ was manually delineated, and large vessels were removed. Vessel density in eight concentric rings with increments of 200-μm diameters from the delineated FAZ was measured. FAZ parameters were calculated using the custom software.

Results. SCP density was significantly lower in the superior (mean difference [MD] = −4.32, 95% confidence interval [CI] = −7.02, −1.61, $P = 0.003$) and nasal (MD = −3.00, 95% CI = 05.22, −0.77, $P = 0.010$) quadrants in XFG versus POAG. SCP vessel density using the concentric ring approach revealed significantly decreased values at all eight rings in XFG versus POAG. In the full-thickness analysis, density was significantly less in the XFG group in all rings except the initial 200 μm. No significant differences existed in FAZ parameters between the groups.

Conclusions. Despite the presence of comparable central visual field defects, the macula vessel density was predominately lower in XFG compared with POAG in our sample of patients. Further studies are warranted to investigate the consistency of our results.

Keywords: exfoliation syndrome, exfoliation glaucoma, optical coherence tomography angiography, superficial capillary plexus, deep capillary plexus, XFG, POAG, OCTA

Glaucoma is a progressive neurodegenerative disorder characterized by retinal ganglion cell (RGC) loss and poses a major risk to global public health. Primary open-angle glaucoma (POAG) is the most common type of glaucoma in the United States.[1] Risk factors associated with progression of POAG include advanced age, elevated intraocular pressure (IOP), and positive family history.[2]

Exfoliation syndrome (XFS) is an age-related systemic disorder of the extracellular matrix in which white fibrillogranular material (exfoliation material, XFM), is deposited in different tissues of the body, including the anterior chamber of the eye.[3] It is the most common recognizable cause of open-angle glaucoma worldwide (exfoliation glaucoma, XFG), accounting for the majority of cases in some countries.[4] It is associated with other ocular conditions such as cataract, angle closure, retinal vein occlusion, and zonular fragility. It is also associated with multiple systemic vascular conditions, such as renal artery stenosis and aortic aneurysm, as well as cerebrovascular and cardiovascular disease, hearing loss, and elastic tissue disorders, such as pelvic organ prolapse, inguinal hernia, and chronic obstructive pulmonary disease.[5–10]

In the eye, XFM is deposited most prominently on the anterior lens surface. Contact between the iris and lens during pupillary movement results in the XFM being scraped off the lens surface and trapped in the trabecular meshwork aqueous outflow pathway. At the same time, the XFM on the lens disrupts the iris pigment epithelium, leading to pigment dispersion and deposition of pigment particles throughout the anterior segment and in the trabecular meshwork. This combination leads to reduction in aqueous outflow capacity and elevated IOP. About 30% of persons with XFS will develop XFG, which is associated with a more severe prognosis compared with POAG.[11]

Optical coherence tomography (OCT) has provided insight into anatomic changes of the optic disc and peripapillary area, such as thinning of the retinal nerve fiber layer (RNFL), the basic defect in glaucoma resulting from loss of retinal ganglion cells.[12] Glaucomatous damage to the macula, which contains the highest concentration of RGCs, has been well documented in recent studies.[13,14] Vascular dysregulation and blood flow abnormalities may play a vital role in the pathogenesis and development of glaucoma as well.[15,16] Decrease in retinal blood flow in POAG using Doppler-Fourier domain OCT,[17] color Doppler,[18] and

scanning laser Doppler flowmetry have been found.[19] Dysregulated retrobulbar[20] and choroidal blood flow have been noted in eyes with POAG.[21] Eyes with exfoliation syndrome have demonstrated impaired ocular perfusion pressure and retrobulbar hemodynamics,[22] impaired posterior ciliary circulation,[23] and altered ophthalmic artery blood flow velocity as well.[24]

OCT angiography (OCTA) is a noninvasive imaging modality that measures blood vessel density at the optic disc and macula by detecting red blood cell movement[25] with great precision and repeatability. OCTA studies have shown agreement between areas of decreased vessel density and areas of visual field defect.[26–28] Decreased vessel density around the optic disc and macula and vascular changes at the foveal avascular zone (FAZ) capillary arcade in patients with POAG have been described.[29–32] The FAZ in healthy eyes often has a circular or elliptical shape, but loss of this circular contour may signify vascular loss and may indicate disease progression in vascular maculopathies.[33–35]

Recent studies have examined peripapillary vessel density using OCTA and demonstrated significantly decreased perfused vessel density in XFG compared to POAG.[36,37] To date, there have been, to our knowledge, no published studies using OCTA to explore changes of the vasculature at the macula in XFG. We chose to investigate the possible vascular differences between POAG and XFG, as observed using OCTA, by looking specifically at macular vessel density and FAZ changes.

Methodology

Participants

This partly retrospective, partly prospective cross-sectional study was conducted at the New York Eye and Ear Infirmary of Mount Sinai from January 2018 to May 2018 and approved by the Mount Sinai Institutional Review Board. The work was executed in accordance with the Code of Ethics of the World Medical Association (Declaration of Helsinki). Written informed consent was obtained from all prospective participants. Retrospective patient data were obtained from screening of the medical charts of participants who had obtained OCTA as part of the standard of care in a private glaucoma practice. Twenty-six patients with XFG and 28 with POAG were included in the study. We retrospectively enrolled 21 XFG patients and 20 POAG patients. We prospectively recruited five XFG patients and eight POAG patients. Only one eye from each patient was selected. If both eyes exhibited the pathology, one eye was randomly selected.

All participants underwent a comprehensive ophthalmic examination, which included assessment of visual acuity, IOP measurement by Goldmann applanation tonometry, slit lamp examination of the anterior segment, and inspection of the optic nerve via ophthalmoscopy. POAG eyes were defined by clinical findings consistent with glaucomatous optic neuropathy, such as vertical cup-to-disc ratio $\geq$0.6, asymmetry of cup-to-disc ratio $\geq$0.2 between eyes, and presence of localized RNFL or neuroretinal rim defects in the absence of any other abnormalities that could explain the findings on fundus examination and open anterior chamber angles. Glaucomatous eyes had glaucoma hemifield test results outside normal limits on at least two consecutive reliable examinations. We defined defects as a minimum of three abnormal points clustered in the same hemifield with a pattern deviation of $<$2% with at least one point of $<$1% or at least two adjacent points with a pattern deviation of $<$1%. XFG eyes had glaucomatous optic neuropathy along with exfoliation material deposition on the anterior lens capsule and/or pupillary margin. There was no washout period before OCTA imaging due to the severity of the glaucomatous damage in some of these cases not allowing for the withdrawal of therapy. IOP was recorded while the patients were using their antiglaucoma medications and was measured on the day of OCTA imaging.

Inclusion criteria required that glaucoma patients had reliable and reproducible defects on perimetry (Humphrey Visual Field 24-2 and 10-2; Carl Zeiss Meditec, Dublin, CA, USA). Patients were included if criteria for both visual field examinations were met, including fixation losses $\leq$33%, false positives $<$15%, and false negatives $<$20%. Glaucoma patients were classified by stage based on 24-2 perimetry: mild was defined as mean deviation (MD) greater than −6 decibels (dB), moderate as −6 to −12 dB, and severe as less than −12 dB.

Exclusion criteria included presence of retinal vaso-occlusive diseases such as retinal arterial/vein occlusion, optic nerve head pathology, hypertensive retinopathy, diabetic retinopathy, age-related macular degeneration, pathological myopia with epiretinal membrane, macular hole, retinal detachment, and/or best corrected visual acuity $>$20/50.

Optical Coherence Tomography Angiography

OCTA images were obtained with a commercial spectral domain-OCT system (Angiovue RTvue; Optovue, Inc., Fremont, CA, USA). Each patient underwent a single imaging session of a 3 $\times$ 3-mm volumetric macular scan (AngioRetina mode). Three volumetric raster scans were taken sequentially and consisted of a horizontal (x-fast) and vertical (y-fast) scan.[32] Each raster scan consisted of 304 B-scans, and each scan was performed twice for a total of 608 B-scans. Each B-scan consisted of 304 A-scans with a rate of 70,000 A-scans per second using a light source of 840 nm.

Images of the perfused vessels were produced using the split spectrum amplitude-decorrelation angiography algorithm, which allowed decreased scan time and improved signal-to-noise ratio of flow reading.[25] Additional built-in Optovue, Inc. software segmented the cross-sectional OCT retinal image into distinct layers. Vasculature investigated included the superficial and deep capillary plexus of the macula. The superficial capillary plexus consisted of vessels from the inner limiting membrane (ILM) to the posterior margin of the inner plexiform layer (IPL). The deep capillary plexus consisted of capillaries between the posterior IPL margin and posterior boundary of the outer plexiform layer. Eyes with poor OCTA image quality, including a signal strength index (SSI) $<$50, significant motion artifacts, media opacity blocking vessel signal, or segmentation error causing poor outline of vascular network, were excluded.

OCTA Image Analysis

Two forms of analysis were used for quantification of the OCTA images. Built-in Angioanalytics software (AngioRetina mode; Optovue, Inc.) analyzed the 3 $\times$ 3-mm superficial capillary plexus (SCP) image obtained and calculated macula vessel density (MVD) percentage based on quadrant segments. The OCTA mapping provided analysis of density in areas based on the Early Treatment Diabetic Retinopathy Study with the foveal center being detected and an annular parafoveal ring with an outer diameter of 2.5 mm and inner diameter of 1.0 mm. This was then divided into quadrants: superior, inferior, nasal, and temporal areas (Fig. 1). This ring was divided into two regions in the superior and inferior hemifield.[38] This quadrant-based approach allowed calculation of density in all these specific areas.

The second form of analysis was done using custom software (MATLAB; The MathWorks, Inc., Natick, MA, USA). First, SCP and deep capillary plexuses (DCP) OCTA scans (between ILM and 70 μm below the posterior margin of the IPL) centered at the fovea were superimposed as previously described[34,39] using MATLAB and were used for image analysis, allowing for the creation of a full-thickness angiogram of the inner retina (Fig. 2A). The

Investigative Ophthalmology & Visual Science

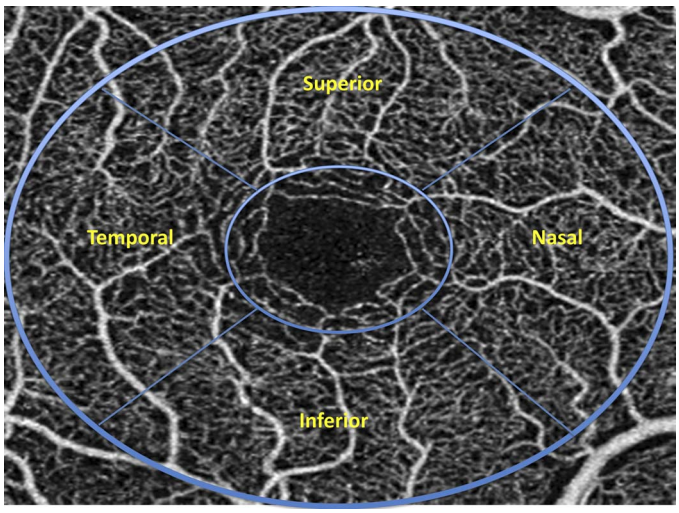

Figure 1. Diagram showing the different quadrants analyzed by built-in software, including superior, temporal, inferior, and nasal quadrants.

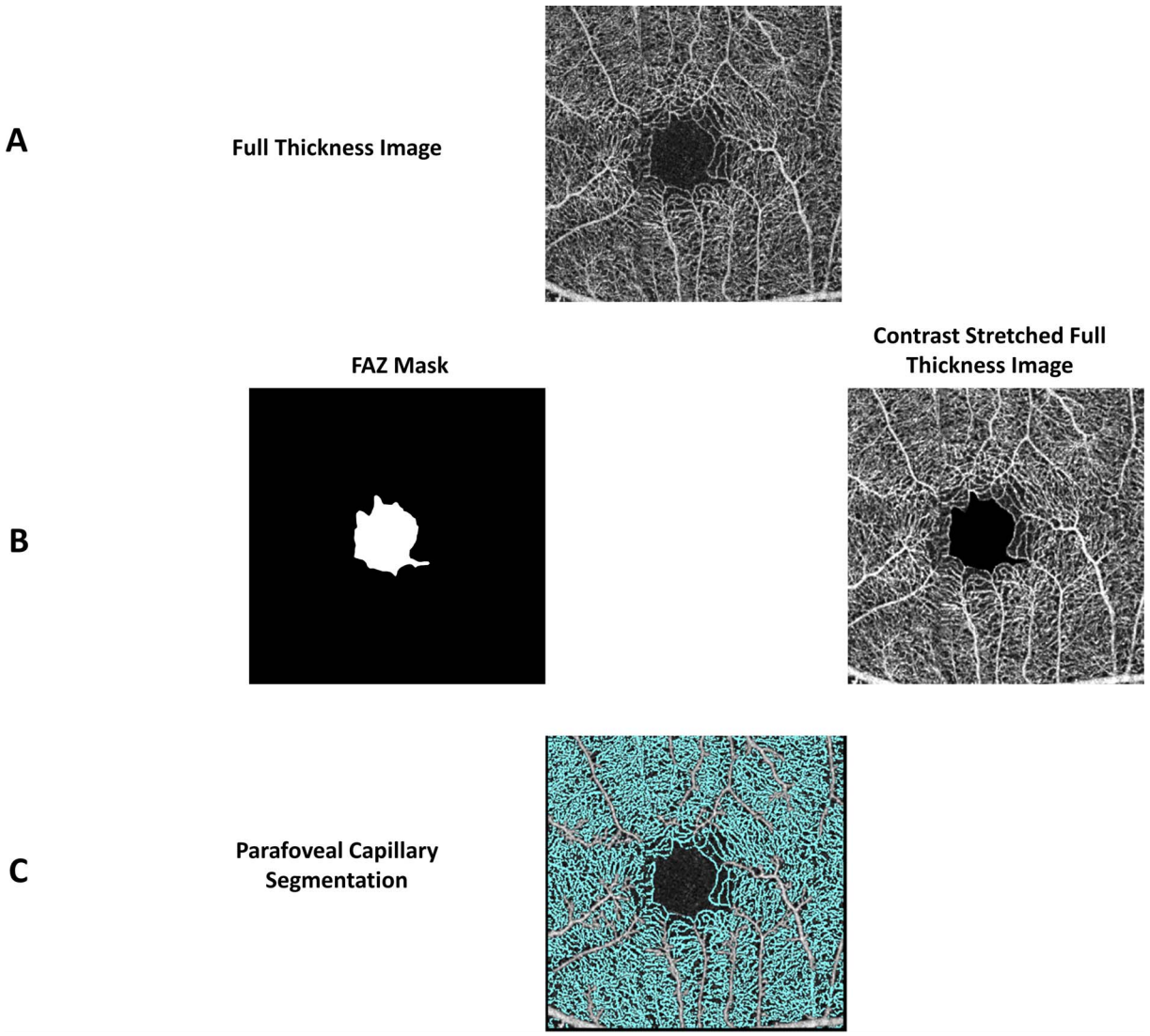

Figure 2. (A) Full-thickness image (between ILM and 70 µm below the posterior margin of the IPL). (B) Delineated FAZ mask with contrast-stretched full-thickness image. (C) Local thresholding for segmenting parafoveal perfused capillaries.

Investigative Ophthalmology & Visual Science

software resized the original image (304 × 304 pixels) by a factor of 6 (1824 × 1824 pixels). The FAZ margin of the full-thickness image was then manually demarcated using a raster graphics editor (Adobe Photoshop; Adobe Systems, Inc., San Jose, CA, USA) by a skilled grader (SP). A second skilled grader (AN) graded a subset of random images from each group to establish intergrader agreement evaluation for FAZ measurement. This random subset consisted of 10 images from the XFG group and 10 from the POAG group. After assigning each eye an ID, a software's random function (Excel; Microsoft, Inc., Bellevue, WA, USA) was used to randomly generate 10 eyes from each group that was graded.

In order to calculate capillary perfusion density at the macula, large retinal vessels (noncapillaries) were recognized and removed using the software. Large vessels were detected by MATLAB on the contrast-stretched resized OCTA image by substituting all pixel intensity >0.7 with value 1 (white) and the remaining pixels with the value 0 (black) using global thresholding. The generated binary mask was then used to eliminate the pixels correlated with the large vessels on the full OCTA image to allow density quantification of the isolated capillaries alone (Fig. 2B). Local thresholding was performed as previously described[40,41] in order to segment parafoveal perfused capillary vasculature (Fig. 2C).

Eight sequential distance concentric rings (200-μm width for each ring) were then created, starting 200 μm from the border of the delineated FAZ on a color-coded parafoveal capillary density map. Rings were then sequentially created at 400, 600, 800, 1000, 1200, 1400, and 1600 μm away from the FAZ. The software corrected for the retinal magnification caused by refractive error by using individual eye axial length obtained from each patient.[42–44] Parafoveal vessel density percentage was calculated for each of the sequential distance rings by the formula:

$$\text{Parafoveal capillary density, \%} = \left(\frac{\text{Parafoveal capillary area}}{\text{Annulus area} - \text{large vessel area}}\right) \times 100$$

SCP density alone was also assessed individually using the same ring-based method described above without superimposition of the two separate layers.

A FAZ mask was created from the demarcated FAZ and used to calculate FAZ parameters, including area, perimeter, equivalent diameter, and acircularity index as previously described (Fig. 2B).[39] We graded FAZ shape acircularity by using the acircularity index, which is defined as the ratio of the perimeter of the delineated FAZ to the perimeter of a circle with an equal area.[39,45] A perfect circle would be defined to have an acircularity index of 1. Aberration of the FAZ circularity (eccentricity) leads to an increase in the index value of >1. Manual measurement/segmentation of the FAZ and the FAZ parameter calculations have been previously described in several studies.[34,39,45,46]

Statistical Analysis

Statistical analyses were performed using statistical software (STATA ver. 15.1; StataCorp., College Station, TX, USA). ANOVA and Kruskal-Wallis testing were used to analyze differences in patient demographic and clinical characteristics. Multiple linear regression analyses were used to evaluate the correlation between MVD percentage data in each area and diagnosis. The same analysis was done to analyze the eight concentric rings and FAZ parameter measurements among the diagnostic groups in both full-thickness and superficial images. Multivariable analysis was done to adjust for age, stage of glaucoma, race, and SSI of OCTA image. $P < 0.05$ was considered statistically significant.

Table 1. Clinical and Demographic Data Across Control, XFS, XFG, and POAG Groups Analyzed Using ANOVA

Variables	XFG, $N = 26$	POAG, $N = 28$	P Value
Age, y, mean ± SD	71.91 ± 6.37	64.52 ± 9.39	0.002
Sex, *n* (%)			0.413
Female	12 (46.15)	17 (60.71)	
Male	14 (53.85)	11 (39.29)	
Race (%)			0.002
Caucasian	25 (96.15)	16 (57.14)	
Black	0	1 (3.57)	
Asian Indian	0	5 (17.86)	
East Asian	0	4 (14.29)	
Hispanic	1 (3.85)	2 (7.14)	
IOP, mean ± SD	16.12 ± 4.52	13.65 ± 4.74	0.061
Pachymetry	548.59 ± 37.06	546.25 ± 30.10	0.858
Stage (%)			0.531
Mild	13 (50.0)	11 (40.74)	
Moderate	5 (19.23)	9 (33.33)	
Severe	8 (30.77)	7 (25.93)	
SSI	64.40 ± 5.32	66.41 ± 8.50	0.317
Axial length	24.12 ± 1.51	25.10 ± 1.87	0.040

SSI indicates signal strength index of OCTA image.

Results

A comprehensive analysis of participants' demographic and clinical characteristics is shown in Table 1. Race was significantly different between the groups ($P < 0.001$). Difference in sex (among all groups) and stage of disease (between XFG and POAG) did not reach statistical significance. Additionally, no statistically significant differences existed between XFG and POAG groups in visual field, MD, and pattern standard deviation (PSD) in both 10-2 and 24-2 protocols after correcting for age ($P > 0.05$; Table 2). Difference in SSI of OCTA images between groups did not reach statistical significance ($P = 0.317$).

The XFG group had statistically significantly lower MVD in the SCP in all areas (inferior, superior, nasal, temporal quadrants, and superior and inferior hemifields) compared to the POAG group. This significance persisted when corrected for age, stage, axial length, race, and SSI, except in the inferior and temporal areas (Table 3). Ring-based SCP MVD analysis showed statistically significant differences between the XFG group and POAG group in all eight concentric rings, with the significance becoming more prominent after correction for age, stage, race, and SSI (Table 4).

Ring-based MVD analysis of the combined full-thickness layer (superimposed SCP + DCP) showed the XFG group had statistically significant lower MVD in all concentric rings except the initial 200-μm ring when corrected for age, stage, race, and SSI ($P = 0.107$; Table 5; Fig. 3).

Analysis of FAZ indices showed no statistically significant differences between the two groups (Table 6). A subset of random FAZ parameters was measured by a second masked grader (AN) in order to assess for intergrader correlation and revealed coefficients of correlation (ICC) = 0.98 (95% confidence interval [CI] = 0.91–1.00). This subset of images was assessed by one grader (SP) and revealed a repeatability coefficient of 0.011 (95% CI = 0.008–0.015) with a measurement error of 0.007.

Investigative Ophthalmology & Visual Science

Table 2. MD and PSD Between XFG and POAG

	Unadjusted			Adjusted for Age		
XFG vs. POAG*	MD	95% CI	*P* Value	MD	95% CI	*P* Value
MD-10	+0.86	−2.42, +4.15	0.600	+1.28	−2.72, +5.28	0.523
PSD-10	−2.91	−5.40, −0.41	0.023	−2.28	−5.25, +0.69	0.129
MD-24	−1.59	−5.27, +2.10	0.391	−1.78	−6.16, +2.59	0.416
PSD-24	−1.66	−4.04, +0.72	0.167	−0.98	−3.81, +1.85	0.489

* 10 = 10-2 visual field perimetry; 24 = 24-2 visual field perimetry. CI, confidence interval.

Discussion

Recent studies have demonstrated lower peripapillary vessel density at the optic in XFG compared to POAG despite comparable visual fields.[36,37,47] We compared MVD in XFG and POAG patients with defects on both 10-2 and 24-2 field perimetry. There were no significant differences between these groups in the PSD and MD in either case, allowing for analysis of groups with comparable visual fields. The usage of 10-2 visual fields also allowed more precise measurement of central vision, which is often involved in macula damage.[48] In our analysis, age and race were significantly different between the two groups ($P < 0.0001$), and this was mainly due to the older population of XFG, as this disorder is age-related and there is a high percentage of Caucasians (96.15%) in that population.[11] Therefore, we controlled for both age and race in our multivariable analysis.

When comparing MVD between XFG and POAG, we found significantly lower SCP MVD at superior and nasal quadrants in

Table 3. Quadrant-Based SCP MVD Analysis at Quadrants using Multivariable Linear Regression Analysis (XFG versus POAG)

XGF vs. POAG	Mean Difference	95% CI	*P* Value
Unadjusted			
MVD sup hemi	−3.28	−5.30, −1.26	0.002
MVD inf hemi	−2.75	−4.97, −0.53	0.016
MVD sup quad	−4.00	−6.35, −1.64	0.001
MVD inf quad	−3.11	−5.66, −0.56	0.018
MVD temp quad	−2.40	−4.20, −0.59	0.010
MVD nasal quad	−3.79	−5.76, −1.82	<0.001
Model 1*			
MVD sup hemi	−2.71	−4.71, −0.71	0.009
MVD inf hemi	−2.41	−4.42, −0.40	0.020
MVD sup quad	−3.95	−6.41, −1.48	0.002
MVD inf quad	−2.68	−5.24, −0.12	0.041
MVD temp quad	−1.69	−3.45, +0.08	0.061
MVD nasal quad	−3.01	−4.99, −1.04	0.004
Model 2†			
MVD sup hemi	−2.72	−4.84, −0.60	0.013
MVD inf hemi	−2.37	−4.49, −0.25	0.029
MVD sup quad	−4.10	−6.69, −1.51	0.003
MVD inf quad	−2.64	−5.34, +0.07	0.056
MVD temp quad	−1.57	−3.44, +0.30	0.097
MVD nasal quad	−2.86	−4.88, −0.83	0.007
Model 3‡			
MVD sup hemi	−3.31	−5.50, −1.12	0.004
MVD inf hemi	−2.84	−5.06, −0.63	0.013
MVD sup quad	−4.90	−7.51, −2.29	<0.001
MVD inf quad	−3.37	−6.13, −0.61	0.018
MVD temp quad	−1.69	−3.67, +0.28	0.091
MVD nasal quad	−3.36	−5.44, −1.28	0.002
Model 4§			
MVD sup hemi	−2.94	−5.23, −1.12	0.013
MVD inf hemi	−2.55	−4.92, −0.19	0.035
MVD sup quad	−4.32	−7.02, −1.61	0.003
MVD inf quad	−2.82	−5.72, +0.09	0.057
MVD temp quad	−1.53	−3.68, +0.61	0.156
MVD nasal quad	−3.00	−5.22, −0.77	0.010

sup, superior; inf, inferior; temp, temporal; hemi, hemifield.
* Model 1 = adjusted for age and SSI.
† Model 2 = adjusted for age, SSI, and stage.
‡ Model 3 = adjusted for age, SSI, stage, and axial length.
§ Model 4 = adjusted for age, SSI, stage, axial length, and race.

Table 4. Ring-Based Annulus Ring MVD of SCP at 200-, 400-, 600-, 800-, 1000-, 1200-, 1400-, and 1600-µm Distance Concentric Rings Using Multivariable Linear Regression Analysis (XFG versus POAG)

XFG vs. POAG, µm	Mean Difference	95% CI	*P* Value
Unadjusted			
200	−3.74	−6.20, −1.28	0.004
400	−5.99	−8.87, −3.12	<0.001
600	−5.68	−8.91, −2.45	0.001
800	−6.81	−10.10, −3.51	<0.001
1000	−7.81	−11.34, −4.28	<0.001
1200	−8.03	−11.62, −4.44	<0.001
1400	−8.91	−12.44, −5.39	<0.001
1600	−7.36	−10.94, −3.79	<0.001
Model 1*			
200	−3.36	−5.85, −0.86	0.010
400	−5.75	−8.83, −2.67	<0.001
600	−5.69	−8.98, −2.39	0.001
800	−6.89	−10.12, −3.66	<0.001
1000	−7.57	−11.25, −3.89	<0.001
1200	−7.47	−11.12, −3.83	<0.001
1400	−8.42	−12.03, −4.81	<0.001
1600	−6.87	−10.66, −3.08	0.001
Model 2†			
200	−3.38	−6.01, −0.75	0.013
400	−5.86	−9.01, −2.72	0.001
600	−5.66	−8.98, −2.34	0.001
800	−7.02	−10.32, −3.72	<0.001
1000	−7.70	−11.40, −4.00	<0.001
1200	−2.31	−11.25, −4.01	<0.001
1400	−8.66	−12.26, −5.06	<0.001
1600	−7.09	−10.77, −3.43	<0.001
Model 3‡			
200	−3.68	−6.53, −0.82	0.013
400	−6.11	−9.51, −2.70	0.001
600	−5.94	−9.46, −2.41	0.002
800	−7.51	−10.93, −4.08	<0.001
1000	−8.51	−12.24, −4.77	<0.001
1200	−8.62	−12.24, −4.99	<0.001
1400	−9.71	−13.29, −6.13	<0.001
1600	−8.64	−12.33, −4.95	<0.001

* Model 1 = adjusted for age and SSI.
† Model 2 = adjusted for age, SSI, and stage.
‡ Model 2 = adjusted for age, SSI, stage, and race.

Investigative Ophthalmology & Visual Science

Table 5. Ring-Based Annulus Ring MVD of Full-Thickness Capillary Plexus at 200-, 400-, 600-, 800-, 1000-, 1200-, 1400-, and 1600-µm Distance Rings Using Multivariable Linear Regression Analysis (XFG versus POAG)

XFG vs. POAG, µm	Mean Difference	95% CI	*P* Value
Unadjusted			
200	−3.86	−6.70, −1.03	0.009
400	−6.90	−9.94, −3.86	<0.001
600	−6.63	−9.61, −3.64	<0.001
800	−7.49	−10.79, −4.20	<0.001
1000	−8.51	−12.14, −4.88	<0.001
1200	−8.89	−12.71, −5.07	<0.001
1400	−9.40	−13.20, −5.60	<0.001
1600	−7.62	−12.03, −3.22	0.001
Model 1*			
200	−2.55	−5.49, +0.40	0.088
400	−5.54	−8.98, −2.09	0.002
600	−5.54	−8.75, −2.32	0.001
800	−6.36	−9.84, −2.87	0.001
1000	−7.22	−11.08, −3.36	<0.001
1200	−7.28	−11.29, −3.27	0.001
1400	−7.83	−11.99, −3.67	<0.001
1600	−5.83	−10.89, −0.79	0.024
Model 2†			
200	−2.78	−5.89, +0.33	0.078
400	−5.87	−9.48, −2.26	0.002
600	−5.73	−9.09, −2.37	0.001
800	−6.61	−10.28, −2.94	0.001
1000	−7.41	−11.49, −3.34	0.001
1200	−7.49	−11.69, −3.29	0.001
1400	−8.01	−12.38, −3.63	0.001
1600	−5.95	−11.28, −0.62	0.030
Model 3‡			
200	−2.75	−6.13, +0.63	0.107
400	−5.62	−9.62, −1.63	0.007
600	−5.74	−9.44, −2.04	0.003
800	−6.74	−10.82, −2.66	0.002
1000	−7.86	−12.35, −3.36	0.001
1200	−8.06	−12.68, −3.44	0.001
1400	−8.56	−13.39, −3.74	0.001
1600	−7.09	−12.83, −1.34	0.017

* Model 1 = adjusted for age and SSI.
† Model 2 = adjusted for age, SSI, and stage.
‡ Model 2 = adjusted for age, SSI, stage, and race.

the XFG group using the quadrant-based approach, but not at the inferior and temporal quadrants. The inferior quadrant of the macula, the inferior vulnerability zone, is more prone to glaucomatous damage, whereas the superior portion may be more resistant to damage.[14] Thus, it seems when considering age, stage, race, and SSI, the inferior macula may be equally affected in both XFG and POAG. Once the threshold of damage is reached in this susceptible area, the capillary loss, manifested as decreased vessel density in the OCTA scan, may be indistinguishable. On the contrary, the vessel density of the superior quadrant that is more resistant to glaucomatous damage is significantly lower in XFG as opposed to POAG, possibly revealing more extensive damage in XFG. The temporal quadrant also may be susceptible to damage, as this area corresponds partly to the inferior vulnerability zone and may explain the lack of significant difference between XFG and POAG. The nasal and superior quadrants maintained significant differences between groups in both univariable and all multivariable analysis.

Table 6. Analysis of FAZ Parameter Differences in XFG Compared to POAG Using Multivariable Linear Regression Analysis

XFG vs. POAG	Mean Difference	95% CI	*P* Value
Unadjusted			
FAZ area	−0.02	−0.08, +0.04	0.410
FAZ perimeter	+0.09	−0.24, +0.42	0.591
FAZ equivalent diameter	+0.09	−0.24, +0.42	0.591
Acircularity index	+0.09	−0.03, +0.20	0.147
Model 1*			
FAZ area	+0.02	−0.04, +0.09	0.491
FAZ perimeter	+0.26	−0.14, +0.66	0.196
FAZ equivalent diameter	+32.69	−39.39, +104.78	0.366
Acircularity index	+0.06	−0.08, +0.20	0.398
Model 2†			
FAZ area	+0.02	−0.05, +0.09	0.516
FAZ perimeter	+0.24	−0.17, +0.65	0.247
FAZ equivalent diameter	+31.41	−42.84, +105.65	0.398
Acircularity index	+0.05	−0.10, +0.20	0.487
Model 3‡			
FAZ area	+0.03	−0.04, +0.11	0.363
FAZ perimeter	+0.30	−0.14, +0.74	0.180
FAZ equivalent diameter	+44.15	−35.06, +123.36	0.266
Acircularity index	+0.05	−0.11, +0.22	0.504

* Model 1 = adjusted for age and SSI.
† Model 2 = adjusted for age, SSI, and stage.
‡ Model 2 = adjusted for age, SSI, stage, and race.

Using our concentric ring-based analytic approach, we found lower SCP MVD in XFG compared to POAG in all eight concentric distance rings. The macula contains the highest RGC density that abides in the inner retinal layer and obtains its oxygen supply from the superficial retinal capillary plexus.[49,50] Decreased vessels may signify damage and loss of nourishment to tissue. MVD at the SCP has been found to be decreased in various studies of patients with POAG[27,51] and in glaucomatous patients with single-hemifield defects.[28] Xu et al. also found more capillary dropout and vessel density at the macula in both early and advanced POAG, with vessel dropout also correlating with areas of 10-2 visual field defects.[52] Our studies confirm lower MVD in glaucoma and also are the first, to our knowledge, to report lower SCP MVD in XFG compared to POAG.

Combined thickness (SCP + DCP) analysis used the concentric ring–based approach and revealed significantly decreased MVD in XFG compared to POAG at all annuli except for the initial 200-µm ring. This is likely due to more severe damage occurring in both glaucomas at this central 200-µm area of the macula, which is supplied only by a single parafoveal ring.[53] Overall, our results may indicate a more prominent vascular change in XFG when compared to POAG in both superficial and deep plexus. XFG is also known to be a more severe glaucoma with higher pressures and faster progression, further explaining the greater loss of vasculature.[11]

To our knowledge, no other studies have examined the FAZ in XFG. We found a higher average FAZ acircularity index and perimeter in XFG compared to POAG (1.50 ± 0.27 vs. 1.41 ± 0.13 and 2.91 ± 0.59 vs. 2.82 ± 0.62, respectively), but this difference did not reach statistical significance. Previous studies have explored the effect of POAG on FAZ parameters and its diagnostic ability to detect differences between glaucoma and control eyes. Choi et al.[54] found significantly altered FAZ parameters in glaucoma and stated this may be a biomarker of parafoveal capillary network interference occurring in glaucoma. Kwon et al.[30] found increased acircularity in

Investigative Ophthalmology & Visual Science

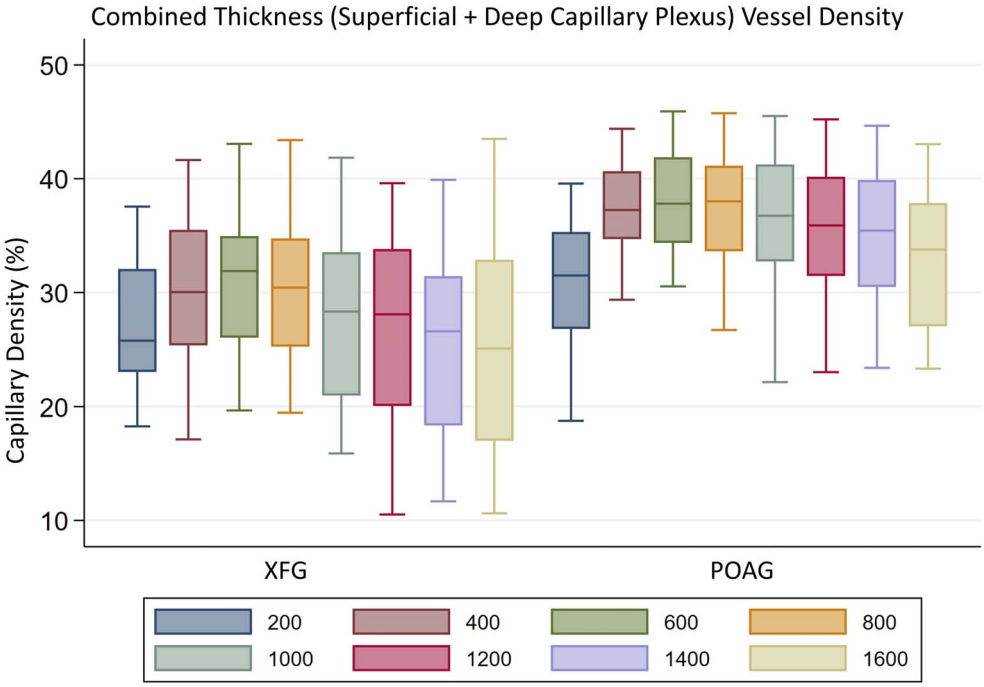

Figure 3. Modified box and whisker plot comparing parafoveal capillary density (%) at the different annular rings (200, 400, 600, 800, 1000, 1200, 1400, and 1600 μm) in combined thickness OCTA images.

patients with central field vision defects. We did not compare our glaucomatous patients with control patients. We did find in our combined thickness analysis that there was no difference in vessel density at the initial central 200-μm annulus, indicting that either there is similar amount of damage to the FAZ perimeter or there was no damage to this zone when comparing POAG versus XFG patients. This may explain the lack of significant difference in our FAZ parameters between groups since after a threshold of damage is reached in the FAZ, change in vessel architecture may be indistinguishable between groups.

Various factors are involved in the pathogenesis of XFS and may explain the changes we found at the macula. Two single nucleotide polymorphisms in the lysyl oxidase-like 1 (*LOXL1*) gene have been found in 99% of Caucasians with XFS. The LOXL1 protein is important for proper cross linkage of collagen and elastin in the extracellular matrix. This enzyme variance may abnormally impact the vascular wall configuration in XFS patients.[7] Accumulation of XFM in tissues may destroy normal cell basement membranes and cause damage known as degenerative fibrillopathy.[55] Over time, the XFM pileup appears to nibble away at the endothelial cells that line blood vessels, as well as the pericytes, contractile cells that wrap around the endothelial cells and help give blood vessel walls strength and flexibility; these cellular changes may impact vascular tissue around the body. XFS may also be associated with compromised autophagy of cellular waste, and this may lead to buildup of misfolded proteins.[56] This abnormality may result in oxidative stress leading to vascular pathology. Clusterin, a chaperone molecule involved in eliminating toxic protein oligomers, likely has altered expression in XFS/XFG, further affecting vascular dysregulation in exfoliation.[57] Additionally, the vasoconstrictive mediator endothelin-1, was found to have higher concentration in the aqueous humor of XFS patients as well.[58] Ischemia, hypoxia, and other biological stress conditions all play a key role in XFS. Decreased antioxidants and increased oxidative markers such as hydrogen peroxide have been found in XFS.[7] The effect of the exfoliation process on ocular vasculature is especially notable at the iris vessels, which show capillary dropout and decreased perfusion as demonstrated by fluorescein angiography.[8] All of these factors may play a role in the vascular dysfunction, leading to lower MVD in XFG.

Our study was not without limitations. One limitation included our small sample size, which may limit the generalizability of our results. Many of our XFG patients were of older age, likely due to exfoliation syndrome being an age-related disorder; however, even after correction for age, our results remained significant. Of importance, the level of damage was comparable between XFG and POAG, as MD and PSD on 10-2 and 24-2 perimetry was not significantly different between the two groups in multivariable analysis (Table 2). Some subjectivity was involved when considering manual delineation of the FAZ margin; however, this was accounted for by usage of an additional grader, which confirmed our ICC = 0.98 (95% CI = 0.91–1.00). This confirms previous studies that found FAZ parameter measurements to have good repeatability in patients with macular conditions.[59,60]

Age is another factor that may have affected the FAZ parameters, but this topic is one of some disagreement. Ghassemi et al.[61] and Samara et al.[62] found no significant difference in mean superficial and deep FAZ area among different age groups. However, Yu et al.[63] found vessel density to decrease and FAZ enlargement to correlate with age. They stated this might be due to tissue loss and thus loss of vascular supply occurring with aging, but it is important to note that this study was limited to a Chinese population. Other studies have demonstrated increased FAZ size with age as well use of fluorescein angiography.[64,65] We did not find significant differences in the FAZ area in our subgroup analysis, but these factors may have been a limitation due to the usage of older patients in our study.

A previous study has demonstrated that the deep vascular plexus density decreases more significantly compared to SCP in glaucoma.[54] Our study did not independently analyze MVD in the DCP due to increased amount of projection artifacts

from the SCP reproducing its vascular layers onto the deep plexus and decreasing its image quality.[25,50] Therefore, we chose to analyze full-thickness vascular layers (superimposed SCPs + DCPs) and the individual SCP layer.

We chose to analyze vessel density using custom and built-in software. The first ring-based analysis is currently achievable only by using the custom software, while the latter is available to clinicians worldwide. We wanted to illustrate demonstrable changes at the macula using both approaches. Ring-based analysis also eliminated the possible effects that large blood vessels (noncapillaries) could have had on MVD measurement, since the software removed these vessels. Additionally, the basis of using circumferential annulus rings around the traced FAZ allowed a more precise assessment of parafoveal density without including possible foveal avascular zone into calculation. We also corrected for SSI of the OCTA images in our study to improve the validity of our results. Although a few studies have made this observation of correlating increased SSI with increased density,[66,67] this step is not taken in many studies that include only an SSI cutoff point. This shortcoming has been recently addressed in a letter to the editor.[68] Correction for SSI is vital, since its effect on image quality, and consequently, MVD is dramatic. Our study was also limited to investigation of glaucomatous eyes with visual field defects on the Humphrey 10-2 protocol, since we wanted to explore the relationship between field defects in the central fixation area in XFG and MVD loss. It is important that we chose 10-2 instead of 24-2 protocols alone since a standard visual field test using a 6° grid often misses the central field loss that may be occurring.[14] Although we did not obtain the RNFL and GCC thickness measurements on our patients due to the mostly retrospective nature of this study, it is important to note that recent studies have observed that MVD was found to be highly associated with the visual field damage and had a comparable diagnostic power on par with peripapillary RNFL and GCC measurements.[51] Additionally, MVD measurements were more associated with glaucomatous damage than were GCC measurements.[69] We did not examine a control group because the differences in MVD between the glaucomatous eyes and the healthy eyes have been shown previously.[27,28,54,70] Also, the main focus of our study was to examine the differences between macular vasculature in XFG and POAG. Despite the small sample size, our study was rigorously controlled for SSI, age, and race, and we used a custom software to eliminate the large blood vessels that could potentially cause overestimation of the vessel density as described above. Lastly, another limitation may have been unknown confounding variables, such as the effect of systemic antihypertensive medications and topical medications on macula perfusion.

The retina and particularly the macular area use more oxygen per weight than any other tissue in the body, thus investigation of the vasculature here is vital.[71] The importance of studying and examining the macula that is important for central fixation cannot be undermined even in early glaucoma.[14] The intimate connection between loss of central fixation used for everyday vision and decline in quality of life is well noted in patients with glaucoma.[72] To the best of our knowledge, our study is the first to show decreased MVD in exfoliation glaucoma when compared to POAG, even after correction for multiple covariables. It is important that the differences were not only at the SCP but also at the full-thickness retina, which included the deep capillary retina plexus. We did not find any differences in FAZ parameters between XFG and POAG, possibly revealing similar damage at the central foveal region. MVD measurement may be useful in tracking progression of glaucomatous patients with central field defects, as we found lower MVD in these glaucomatous patients. In our groups of POAG and XFG patients with central field defects, the lower MVD demonstrated at both the superficial and combined vascular layers of the XFG group compared to the POAG indicates a more severe vascular involvement in XFG and that vessel density analysis may be useful for tracking the damage in patients with central field defects. Our findings may also elucidate a different pathogenesis of damage that may correspond with the more severe nature of exfoliation glaucoma. This finding may emphasize the need for more targeted and aggressive therapy in XFG compared to POAG.

Acknowledgments

Supported by the Crowley Family Fund of the New York Eye and Ear Infirmary of Mount Sinai, New York, New York, United States. The National Eye Institute of the National Institutes of Health under award number R01EY027301. The content is solely the responsibility of the authors and does not necessarily represent the official views of the National Institutes of Health. Additional funding for this research was provided by the New York Eye and Ear Infirmary Foundation Grant, Marrus Family Foundation, the Geraldine Violett Foundation, The Edward N. & Della L. Thome Memorial Foundation, and the Jorge N. Buxton Microsurgical Foundation.

Disclosure: **S. Philip**, None; **A. Najafi**, None; **A. Tantraworasin**, None; **T.Y.P. Chui**, None; **R.B. Rosen**, OD∼OS (C), Guardian Health (C), Boehringer-Ingelheim (C), CellView (C), Diopsys (C), Nano Retina (C), Regeneron (C), Zeavision (C), TEVA (C), Opticology (I), Optovue (I, C); **R. Ritch**, None

References

1. Ritch R, Shields MB, Krupin T. *The Glaucomas*. 2nd ed. St Louis: Mosby; 1996.
2. Leske MC, Heijl A, Hyman L, et al. Predictors of long-term progression in the early manifest glaucoma trial. *Ophthalmology*. 2007;114:1965–1972.
3. Prince AM, Streeten BW, Ritch R, et al. Preclinical diagnosis of pseudoexfoliation syndrome. *Arch Ophthalmol*. 1987;105:1076–1082.
4. Ritch R. Exfoliation syndrome. The most common identifiable cause of open-angle glaucoma. *J Glaucoma*. 1994;3:176–177.
5. Ritch R. Systemic associations of exfoliation syndrome. *Asia Pac J Ophthalmol*. 2016;5:45–50.
6. Wirostko BM, Curtin K, Ritch R, et al. Risk for exfoliation syndrome in women with pelvic organ prolapse: a Utah Project on Exfoliation Syndrome (UPEXS) study. *JAMA Ophthalmol*. 2016;134:1255–1262.
7. Aboobakar IF, Johnson WM, Stamer WD, et al. Major review: exfoliation syndrome; advances in disease genetics, molecular biology, and epidemiology. *Exp Eye Res*. 2017;154:88–103.
8. Helbig H, Schlötzer-Schrehardt U, Noske W, et al. Anterior-chamber hypoxia and iris vasculopathy in pseudoexfoliation syndrome. *Ger J Ophthalmol*. 1994;3:148–153.
9. Gonen KA, Gonen T, Gumus B. Renal artery stenosis and abdominal aorta aneurysm in patients with pseudoexfoliation syndrome. *Eye*. 2013;27:735–741.
10. Besch BM, Curtin K, Ritch R, et al. Association of exfoliation syndrome with risk of indirect inguinal hernia: the Utah project on exfoliation syndrome. *JAMA Ophthalmol*. 2018;136:1368–1374.
11. Ritch R, Schlötzer-Schrehardt U. Exfoliation syndrome. *Surv Ophthalmol*. 2001;45:265–315.
12. Wollstein G, Schuman JS, Price LL, et al. Optical coherence tomography (OCT) macular and peripapillary retinal nerve fiber layer measurements and automated visual fields. *Am J Ophthalmol*. 2004;138:218–225.

13. Leung CKS, Chan WM, Yung WH, et al. Comparison of macular and peripapillary measurements for the detection of glaucoma: an optical coherence tomography study. *Ophthalmology*. 2005;112:391–400.
14. Hood DC, Raza AS, de Moraes CGV, Liebmann JM, Ritch R. Glaucomatous damage of the macula. *Prog Retin Eye Res*. 2013;32:1–21.
15. Pasquale LR. Vascular and autonomic dysregulation in primary open-angle glaucoma. *Curr Opin Ophthalmol*. 2016;27:94–101.
16. Choi J, Kook MS. Systemic and ocular hemodynamic risk factors in glaucoma. *Biomed Res Int*. 2015;2015:141905.
17. Wang Y, Fawzi AA, Varma R, et al. Pilot study of optical coherence tomography measurement of retinal blood flow in retinal and optic nerve diseases. *Invest Ophthalmol Vis Sci*. 2011;52:840–845.
18. Galambos P, Vafiadis J, Vilchez SE, et al. Compromised autoregulatory control of ocular hemodynamics in glaucoma patients after postural change. *Ophthalmology*. 2006;113:1832–1836.
19. Michelson G, Langhans MJ, Groh MJ. Perfusion of the juxtapapillary retina and the neuroretinal rim area in primary open angle glaucoma. *J Glaucoma*. 1996;5:91–98.
20. Kanakamedala P, Harris A, Siesky B, et al. Optic nerve head morphology in glaucoma patients of African descent is strongly correlated to retinal blood flow. *Br J Ophthalmol*. 2014;98:1551–1554.
21. Ulrich A, Ulrich C, Barth T, Ulrich WD. Detection of disturbed autoregulation of the peripapillary choroid in primary open angle glaucoma. *Ophthalmic Surg Lasers*. 1996;27:746–757.
22. Galassi F, Giambene B, Menchini U. Ocular perfusion pressure and retrobulbar haemodynamics in pseudoexfoliative glaucoma. *Graefe's Arch Clin Exp Ophthalmol*. 2008;246:411–416.
23. Detorakis ET, Achtaropoulos AK, Drakonaki EE, et al. Hemodynamic evaluation of the posterior ciliary circulation in exfoliation syndrome and exfoliation glaucoma. *Graefe's Arch Clin Exp Ophthalmol*. 2007;245:516–521.
24. Dayanir V, Topaloğlu A, Ozsunar Y, et al. Orbital blood flow parameters in unilateral pseudoexfoliation syndrome. *Int Ophthalmol*. 2009;29:27–32.
25. Jia Y, Tan O, Tokayer J, et al. Split-spectrum amplitude-decorrelation angiography with optical coherence tomography. *Opt Express*. 2012;20:4710.
26. de Carlo TE, Romano A, Waheed NK, Duker JS. A review of optical coherence tomography angiography (OCTA). *Int J Retina Vitreous*. 2015;1:5.
27. Takusagawa HL, Liu L, Ma KN, et al. Projection-resolved optical coherence tomography angiography of macular retinal circulation in glaucoma. *Ophthalmology*. 2017;124:1589–1599.
28. Yarmohammadi A, Zangwill LM, Diniz-Filho A, et al. Peripapillary and macular vessel density in patients with glaucoma and single-hemifield visual field defect. *Ophthalmology*. 2017;124:709–719.
29. Geyman LS, Garg RA, Suwan Y, et al. Peripapillary perfused capillary density in primary open-angle glaucoma across disease stage: an optical coherence tomography angiography study. *Br J Ophthalmol*. 2017;101:1261–1268.
30. Kwon J, Choi J, Shin JW, et al. Alterations of the foveal avascular zone measured by optical coherence tomography angiography in glaucoma patients with central visual field defects. *Invest Opthalmol Vis Sci*. 2017;58:1637–1645.
31. Bresnick GH, Condit R, Syrjala S, et al. Abnormalities of the foveal avascular zone in diabetic retinopathy. *Arch Ophthalmol*. 1984;102:1286–1293.
32. Liu L, Jia Y, Takusagawa HL, et al. Optical coherence tomography angiography of the peripapillary retina in glaucoma. *JAMA Ophthalmol*. 2015;133:1045–1052.
33. Conrath J, Giorgi R, Raccah D, Ridings B. Foveal avascular zone in diabetic retinopathy: quantitative vs qualitative assessment. *Eye*. 2005;19:322–326.
34. Mo S, Krawitz B, Efstathiadis E, et al. Imaging foveal microvasculature: optical coherence tomography angiography versus adaptive optics scanning light ophthalmoscope fluorescein angiography. *Invest Ophthalmol Vis Sci*. 2016;57:OCT130–OCT140.
35. Parodi MB, Visintin F, Della Rupe P, Ravalico G. Foveal avascular zone in macular branch retinal vein occlusion. *Int Ophthalmol*. 1995;19:25–28.
36. Suwan Y, Geyman LS, Fard MA, et al. Peripapillary perfused capillary density in exfoliation syndrome and exfoliation glaucoma vs POAG and healthy controls: an optical coherence tomography angiography study. *Asia Pac J Ophthalmol*. 2018;7:84–89.
37. Rebolleda G, Pérez-Sarriegui A, De Juan V, Ortiz-Toquero S, Muñoz-Negrete FJ. A comparison of two optical coherence tomography–angiography devices in pseudoexfoliation glaucoma versus primary open-angle glaucoma and healthy subjects [published online ahead of print October 14, 2018]. *Eur J Ophthalmol*. https://doi.org/10.1177/1120672118805882.
38. Grading diabetic retinopathy from stereoscopic color fundus photographs—an extension of the modified airlie house classification: ETDRS Report Number 10. *Ophthalmology*. 1991;98(suppl 5):786–806.
39. Krawitz BD, Mo S, Geyman LS, et al. Acircularity index and axis ratio of the foveal avascular zone in diabetic eyes and healthy controls measured by optical coherence tomography angiography. *Vision Res*. 2017;139:177–186.
40. Andrade JS, Linderman R, Pinhas A, et al. Novel development of parafoveal capillary density deviation mapping using an age-group and eccentricity matched normative OCT angiography database. *Trans Vis Sci Tech*. In press.
41. Rosen RB, Andrade Romo JS, Krawitz BD, et al. Earliest evidence of preclinical diabetic retinopathy revealed using OCT angiography (OCTA) perfused capillary density [published online ahead of print January 25, 2019]. *Am J Ophthalmol*. doi:10.1016/j.ajo.2019.01.012.
42. Sampson DM, Gong P, An D, et al. Axial length variation impacts on superficial retinal vessel density and foveal avascular zone area measurements using optical coherence tomography angiography. *Invest Ophthalmol Vis Sci*. 2017;58:3065–3072.
43. Nakanishi H, Akagi T, Hangai M, et al. Effect of axial length on macular ganglion cell complex thickness and on early glaucoma diagnosis by spectral-domain optical coherence tomography. *J Glaucoma*. 2016;25:e481–e490.
44. Kang SH, Hong SW, Im SK, Lee SH, Ahn MD. Effect of myopia on the thickness of the retinal nerve fiber layer measured by cirrus HD optical coherence tomography. *Invest Ophthalmol Vis Sci*. 2010;51:4075–4083.
45. Linderman R, Salmon AE, Strampe M, et al. Assessing the accuracy of foveal avascular zone measurements using optical coherence tomography angiography: segmentation and scaling. *Trans Vis Sci Tech*. 2017;6(3):16.
46. Shahlaee A, Pefkianaki M, Hsu J, et al. Measurement of foveal avascular zone dimensions and its reliability in healthy eyes using optical coherence tomography angiography. *Am J Ophthalmol*. 2016;161:50–55.
47. Park JH, Yoo C, Girard MJA, et al. Peripapillary vessel density in glaucomatous eyes: comparison between pseudoexfoliation glaucoma and primary open-angle glaucoma. *J Glaucoma*. 2018;27:1009–1016.

48. Traynis I, De Moraes CG, Raza AS, et al. Prevalence and nature of early glaucomatous defects in the central 10° of the visual field. *JAMA Ophthalmol*. 2014;132:291–297.
49. Provis JM. Development of the primate retinal vasculature. *Prog Retin Eye Res*. 2001;20:799–821.
50. Campbell JP, Zhang M, Hwang TS, et al. Detailed vascular anatomy of the human retina by projection-resolved optical coherence tomography angiography. *Sci Rep*. 2017;7:42201.
51. Chen HSL, Liu CH, Wu WC, et al. Optical coherence tomography angiography of the superficial microvasculature in the macular and peripapillary areas in glaucomatous and healthy eyes. *Invest Ophthalmol Vis Sci*. 2017;58:3637–3645.
52. Xu H, Yu J, Kong X, et al. Macular microvasculature alterations in patients with primary open-angle glaucoma A cross-sectional study. *Medicine*. 2016;95:e4341.
53. Weinhaus RS, Burke JM, Delori FC, et al. Comparison of fluorescein angiography with microvascular anatomy of macaque retinas. *Exp Eye Res*. 1995;61:1–16.
54. Choi J, Kwon J, Shin JW, et al. Quantitative optical coherence tomography angiography of macular vascular structure and foveal avascular zone in glaucoma. *PLoS One*. 2017;12:e0184948.
55. Streeten BW, Li ZY, Wallace RN, et al. Pseudoexfoliative fibrillopathy in visceral organs of a patient with pseudoexfoliation syndrome. *Arch Ophthalmol*. 1992;110:1757–1762.
56. Bernstein AM, Ritch R, Wolosin JM. Exfoliation syndrome: a disease of autophagy and LOXL1 proteopathy. *J Glaucoma*. 2018;27(suppl 1):S44–S53.
57. Wiggs JL, Kang JH, Fan B, et al. Role for clusterin in exfoliation syndrome and exfoliation glaucoma? *J Glaucoma*. 2018;27(supp 1):S61–S66.
58. Koliakos GG, Konstas AG, Schlötzer-Schrehardt U, et al. Endothelin-1 concentration is increased in the aqueous humour of patients with exfoliation syndrome. *Br J Ophthalmol*. 2004;88:523–527.
59. Shahlaee A, Samara WA, Hsu J, et al. In vivo assessment of macular vascular density in healthy human eyes using optical coherence tomography angiography. *Am J Ophthalmol*. 2016;165:39–46.
60. Rosenfeld PJ, Durbin MK, Roisman L, et al. ZEISS Angioplex™ spectral domain optical coherence tomography angiography: technical aspects. *Dev Ophthalmol*. 2016;56:18–29.
61. Ghassemi F, Mirshahi R, Bazvand F, et al. The quantitative measurements of foveal avascular zone using optical coherence tomography angiography in normal volunteers. *J Curr Ophthalmol*. 2017;29:293–299.
62. Samara WA, Say EAT, Khoo CTL, et al. Correlation of foveal avascular zone size with foveal morphology in normal eyes using optical coherence tomography angiography. *Retina*. 2015;35:2188–2195.
63. Yu J, Jiang C, Wang X, et al. Macular perfusion in healthy chinese: an optical coherence tomography angiogram study. *Invest Ophthalmol Vis Sci*. 2015;56:3212–3217.
64. Wu LZ, Huang ZS, Wu DZ, et al. Characteristics of the capillary-free zone in the normal human macula. *Jpn J Ophthalmol*. 1985;29:406–411.
65. Laatikainen L. The fluorescein angiography revolution: a breakthrough with sustained impact. *Acta Ophthalmol Scand*. 2004;82:381–392.
66. Venugopal JP, Rao HL, Weinreb RN, et al. Repeatability of vessel density measurements of optical coherence tomography angiography in normal and glaucoma eyes. *Br J Ophthalmol*. 2018;102:352–357.
67. Rao HL, Pradhan ZS, Weinreb RN, et al. Determinants of peripapillary and macular vessel densities measured by optical coherence tomography angiography in normal eyes. *J Glaucoma*. 2017;26:491–497.
68. Holló G. Letter to the Editor to Park J-H et al., Peripapillary vessel density in glaucomatous eyes: comparison between pseudoexfoliation glaucoma and primary open-angle glaucoma." *J Glaucoma*. 2018;28:e35.
69. Shoji T, Zangwill LM, Akagi T, et al. Progressive macula vessel density loss in primary open-angle glaucoma: a longitudinal study. *Am J Ophthalmol*. 2017;182:107–117.
70. Lommatzsch C, Rothaus K, Koch JM, et al. OCTA vessel density changes in the macular zone in glaucomatous eyes. *Graefe's Arch Clin Exp Ophthalmol*. 2018;256:1499–1508.
71. Yu DY, Cringle SJ. Oxygen distribution and consumption within the retina in vascularised and avascular retinas and in animal models of retinal disease. *Prog Retin Eye Res*. 2001;20:175–208.
72. Abe RY, Diniz-Filho A, Costa VP, et al. The impact of location of progressive visual field loss on longitudinal changes in quality of life of patients with glaucoma. *Ophthalmology*. 2016;123:552–557.

Investigative Ophthalmology & Visual Science